Cell Calcium 60 (2016) 256–265

Contents lists available at ScienceDirect

Cell Calcium

journal homepage: www.elsevier.com/locate/ceca

Development of practical red fluorescent probe for cytoplasmic calcium ions with greatly improved cell-membrane permeability

Kazuhisa Hirabayashi[a], Kenjiro Hanaoka[a,*], Takahiro Egawa[a], Chiaki Kobayashi[a], Shodai Takahashi[a], Toru Komatsu[a,b], Tasuku Ueno[a], Takuya Terai[a], Yuji Ikegaya[a], Tetsuo Nagano[c], Yasuteru Urano[a,d,e,*]

[a] Graduate School of Pharmaceutical Sciences, The University of Tokyo, 7-3-1 Hongo, Bunkyo-ku, Tokyo 113-0033, Japan
[b] Precursory Research for Embryonic Science and Technology (PRESTO), Japan Science and Technology Agency (JST), 4-1-8 Honcho, Kawaguchi, Saitama 332-0012, Japan
[c] Drug Discovery Initiative, The University of Tokyo, Tokyo 113-0033, Japan
[d] Graduate School of Medicine, The University of Tokyo, 7-3-1 Hongo, Bunkyo-ku, Tokyo 113-0033, Japan
[e] CREST, AMED, Saitama 332-0012, Japan

ARTICLE INFO

Article history:
Received 12 March 2016
Received in revised form 4 June 2016
Accepted 7 June 2016
Available online 8 June 2016

Keywords:
Calcium
Fluorescence
Imaging
Spectroscopy
Small molecule

ABSTRACT

Fluorescence imaging of calcium ions (Ca^{2+}) has become an essential technique for investigation of signaling pathways involving Ca^{2+} as a second messenger. But, Ca^{2+} signaling is involved in many biological phenomena, and therefore simultaneous visualization of Ca^{2+} and other biomolecules (multicolor imaging) would be particularly informative. For this purpose, we set out to develop a fluorescent probe for Ca^{2+} that would operate in a different color region (red) from that of probes for other molecules, many of which show green fluorescence, as exemplified by green fluorescent protein (GFP). We previously developed a red fluorescent probe for monitoring cytoplasmic Ca^{2+} concentration, based on our established red fluorophore, TokyoMagenta (TM), but there remained room for improvement, especially as regards efficiency of introduction into cells. We considered that this issue was probably mainly due to limited water solubility of the probe. So, we designed and synthesized a red-fluorescent probe with improved water solubility. We confirmed that this Ca^{2+} red-fluorescent probe showed high cell-membrane permeability with bright fluorescence. It was successfully applied to fluorescence imaging of not only live cells, but also brain slices, and should be practically useful for multicolor imaging studies of biological mechanisms.

1. Introduction

The development of sophisticated fluorescent probes has contributed to elucidation of the molecular mechanisms of many complex biological phenomena [1–4]. In particular, fluorescence imaging of Ca^{2+} has become an essential technique for investigation of signaling pathways involving Ca^{2+} as a second messenger. For example, changes in the intracellular Ca^{2+} concentration are related to physiological responses in obesity, as well as immune responses and pathological responses in Alzheimer's disease [5–10]. Because Ca^{2+} signaling is involved in so many biological phenomena [11,12], simultaneous visualization of Ca^{2+} and other biomolecules, that is, multicolor imaging, would be particularly informative for detailed study of the mechanisms.

Fluorescent Ca^{2+} indicators can be categorized into two main classes: those based on genetically encoded fluorescent proteins [13,14] and those based on fluorescent small organic molecules [5]. Both types of indicators have characteristic advantages and disadvantages; for example, small-molecular probes have the particular advantage that their AM ester form (cell-permeable acetoxymethyl ester derivative) can be readily bulk-loaded into live cells with no need for transfection. Most currently used small-molecular fluorescent probes for Ca^{2+} are fluorescein derivatives, such as Fluo-3, Fluo-4, Calcium Green-1, and Oregon Green 488 BAPTA-1, and emit green fluorescence (ca. 527 nm) [15–17]. There are also some red-emitting fluorescent probes for Ca^{2+}, such as Rhod-2 (ca. 576 nm), which is a rhodamine derivative [15]. These red-emitting fluorescent probes for Ca^{2+}, including Rhod-2, are widely used for

Abbreviations: TM, TokyoMagenta; AM, acetoxymethyl ester.

* Corresponding authors at: Graduate School of Pharmaceutical Sciences, The University of Tokyo, 7-3-1 Hongo, Bunkyo-ku, Tokyo 113-0033, Japan
E-mail addresses: khanaoka@mol.f.u-tokyo.ac.jp (K. Hanaoka), uranokun@m.u-tokyo.ac.jp, urano@mol.f.u-tokyo.ac.jp (Y. Urano).

http://dx.doi.org/10.1016/j.ceca.2016.06.002
0143-4160/

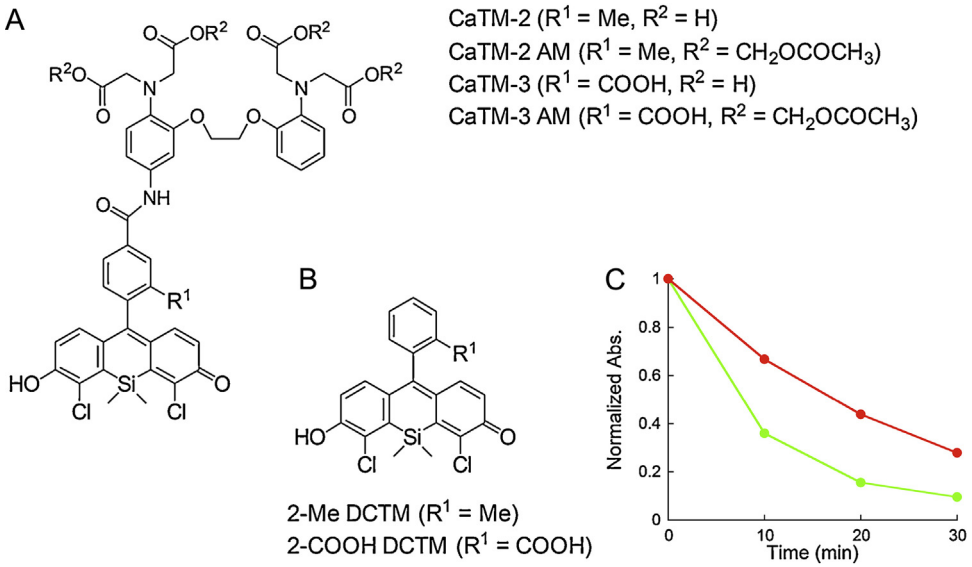

Fig. 1. Chemical structures of fluorescent probes for Ca^{2+}. A. Chemical structures of red fluorescent Ca^{2+} probes, CaTM-2 and CaTM-3, and their cell-permeable derivatives, CaTM-2 AM and CaTM-3 AM. B. Chemical structures of 2-Me DCTM and 2-COOH DCTM [26,27]. C. Photobleaching tests. Normalized absorbance at 482 nm for 1 μM fluorescein (green) and 591 nm for 1 μM 2-COOH DCTM (red). Absorbance measurements were made at 25 °C in 100 mM sodium phosphate buffer at pH 9.0 containing 0.1% DMSO as a cosolvent after samples were exposed to light (30 mW, 470–495 nm for fluorescein, 565–585 nm for 2-COOH DCTM, respectively). (For interpretation of the references to colour in this figure legend, the reader is referred to the web version of this article.)

biological studies, but the cationic nature of the rhodamine scaffold generally causes Rhod-2 AM to localize into mitochondria [18]. Although this behavior is useful for monitoring Ca^{2+} dynamics in mitochondria, visualization of cytoplasmic Ca^{2+} is often much more important for research on Ca^{2+} signaling pathways. Influx of Ca^{2+} into the cytoplasm from the extracellular environment or intracellular stores, such as the endoplasmic reticulum, triggers numerous cellular responses via the interaction of Ca^{2+} with various Ca^{2+}-binding proteins, such as calmodulin and troponin C [11,12]. Fura Red is a representative near-infrared (NIR) fluorescent probe for cytoplasmic Ca^{2+} in biological research, but has the major drawback of extremely low fluorescence quantum efficiency ($\Phi_{fl} \approx 0.013$) [19]. Accordingly, the fluorescence signal is very small unless a high concentration of Fura Red or a high-powered laser is used. However, the use of a high dye concentration has a buffering effect on Ca^{2+}, and the use of a high laser power causes rapid photobleaching of the dye and phototoxicity to the cells.

The red or far-red wavelength region is especially attractive for fluorescence imaging, affording higher tissue penetration due to reduced scattering, low absorption by endogenous biomolecules, and lower phototoxicity, and also allows monitoring of Ca^{2+} in cells or tissues expressing yellow- or green-colored fluorescent proteins or labeled with other green-colored fluorophores [20–22]. Several new red-to-NIR fluorescent probes for cytoplasmic Ca^{2+}, such as Quest Rhod-4 AM, CaSiR-1 [23], KFCA [24], and Calcium Rubies [22,25] have recently been reported [20]. We developed a red (ca. 609 nm) fluorescent probe for monitoring cytoplasmic Ca^{2+}, CaTM-2 and CaTM-2 AM (Fig. 1A), based on the 2-Me DiChloro-TokyoMagenta (2-Me DCTM) scaffold (Fig. 1B) [26]. However, the cell-membrane permeability was limited, and we considered that the low water solubility of the probe was a major contributor to its relatively poor introduction efficiency into cells.

Here, we present a new red-fluorescent Ca^{2+} probe, CaTM-3 AM, with high cell-membrane permeability and bright fluorescence (Fig. 1A). We very recently reported the synthesis and characterization of 2-COOH DCTM (Fig. 1B), which has a carboxy group in place of the methyl group of 2-Me DCTM [27]. Taking account of the high water solubility of 2-COOH DCTM compared with that of 2-Me DCTM, we designed and synthesized CaTM-3 AM as a novel, highly cell-permeable candidate probe for visualization of cytoplasmic Ca^{2+}. We also evaluated its suitability for practical use by employing it for fluorescence imaging of cytoplasmic Ca^{2+} in live cells and in brain slices.

2. Methods

2.1. UV–vis and fluorescence spectra measurements

UV–vis spectra were obtained with a spectrometer (UV-1650, Shimadzu, Japan). Fluorescence spectroscopic studies were performed on a fluorescence spectrometer (F-4500, Hitachi, Japan). The slit width was 2.5 nm for both excitation and emission. The photomultiplier voltage was 700 V. 1 mM dyes in DMSO were used as stock solutions.

2.2. Photobleaching tests

1 μM of dye in 100 mM sodium phosphate buffer at pH 9.0 containing 0.1% DMSO as a cosolvent was poured into the cuvette. The solution was exposed to light (30 mW, 470–495 nm for fluorescein and 565–585 nm for 2-COOH DCTM) through a rod lens using a Xe light source, MAX301 (Asahi Spectra Co., Ltd.) for 30 min. After every 10 min of light irradiation, UV–vis spectra were obtained with a spectrometer (UV-1650, Shimadzu, Japan).

2.3. Relative fluorescence quantum yields

For determination of the relative fluorescence quantum efficiencies (Φ_{fl}) of CaTM-3, 2-Me TM in 0.1 M sodium phosphate buffer (pH 9.0) (Φ_{fl} = 0.42) was used as a standard [28]; calculation was done using Eq. (1):

$$\Phi_x/\Phi_{std} = [A_{std}/A_x][n_x{}^2/n_{std}{}^2][D_x/D_{std}] \quad (1)$$

where std and x represent the standard (2-Me TM) and sample, respectively. A, n, and D are the absorbance at the excitation wave-

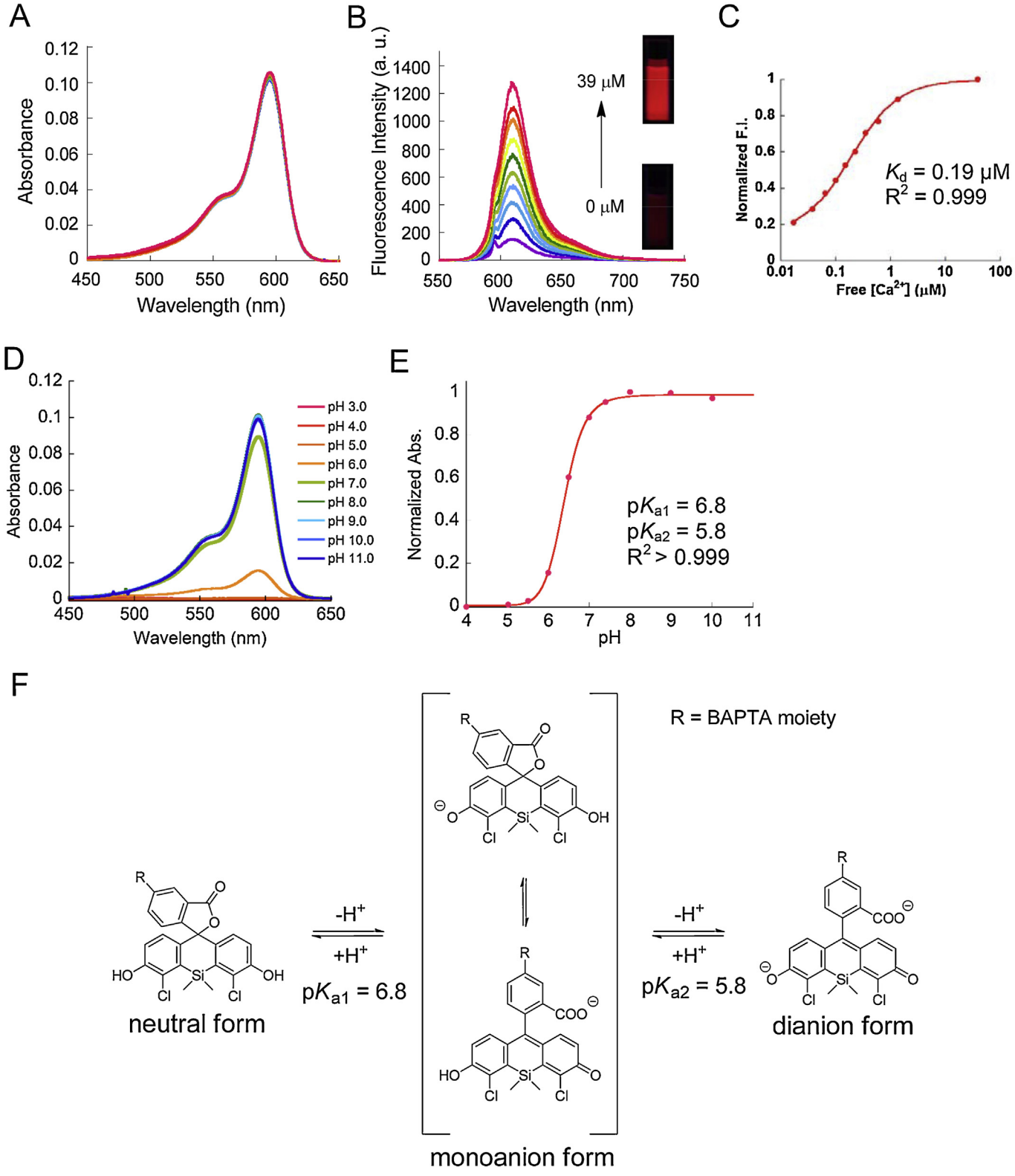

Fig. 2. Photophysical properties of CaTM-3. A. Absorbance and B. emission spectra of 1 μM CaTM-3 in the presence of various concentrations of free Ca^{2+} (0, 0.017, 0.038, 0.065, 0.100, 0.150, 0.225, 0.351, 0.602, 1.35, 39 μM) in 30 mM 3-(*N*-morpholino)propanesulfonic acid (MOPS) buffer containing 100 mM KCl and 10 mM ethyleneglycol tetraacetic acid (EGTA), pH 7.2, at 20 °C. The excitation wavelength was 595 nm. The photographs show the fluorescence of 1 μM CaTM-3 in the presence of 0 μM (bottom) and 39 μM (upper) free Ca^{2+}, and were taken using a handy UV lamp (λ_{ex} = 365 nm). C. Plot of the fluorescence intensities of CaTM-3 at 609 nm in the presence of various concentrations of free Ca^{2+} (μM). The K_d value of CaTM-3 with Ca^{2+} was calculated to be 0.19 μM. D. pH-Dependency of absorption spectra of 1 μM CaTM-3 at 25 °C in 100 mM sodium phosphate buffer at various pH values, containing 1% DMSO as a cosolvent. E. pH Plot of normalized absorbance at 595 nm of CaTM-3. Curve fitting was done with a biphasic equation. The pK_{a1} and the pK_{a2} were calculated to be 6.8 and 5.8, respectively. F. Proposed chemical equilibrium of CaTM-3.

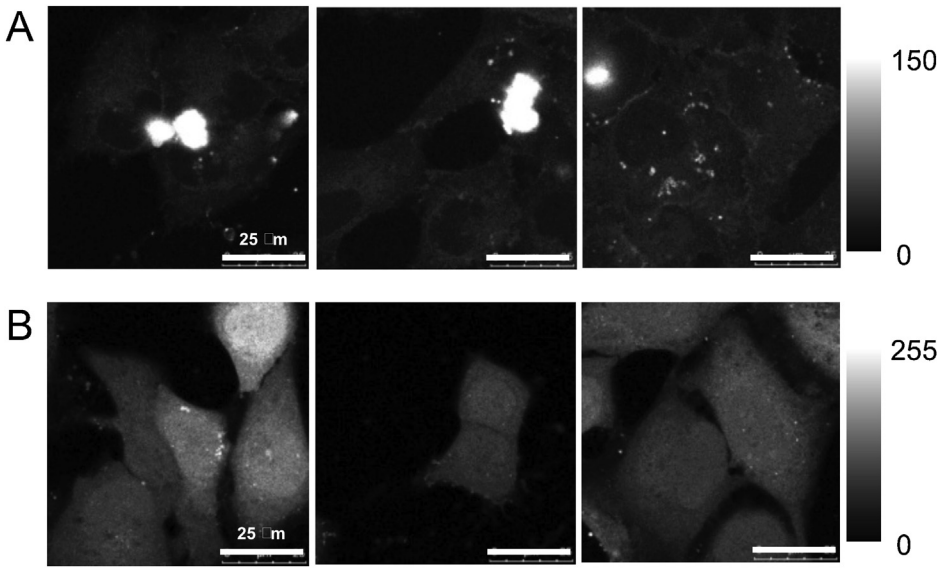

Fig. 3. Comparison between CaTM-2 and CaTM-3 for fluorescence imaging. Fluorescence images of live cells using A. CaTM-2 AM and B. CaTM-3 AM. HeLa cells were incubated with 3 μM CaTM-2 AM or CaTM-3 AM in HBSS buffer containing 0.3% DMSO at 37 °C for 30 min. The dyes were washed out three times and fluorescence images were captured. The excitation and emission wavelengths were 590 nm and 610–680 nm, respectively.

length, refractive index, and area under the fluorescence spectra on an energy scale, respectively.

2.4. Determination of dissociation constant with Ca^{2+}

A Calcium Calibration Buffer Kit (Invitrogen) was used to control free Ca^{2+} concentration. Absorption and emission spectra of 1 μM CaTM-3 were measured in the presence of various concentrations of free Ca^{2+} (0, 0.017, 0.038, 0.065, 0.100, 0.150, 0.225, 0.351, 0.602, 1.35, and 39 μM) in 30 mM 3-(*N*-morpholino)propanesulfonic acid (MOPS) buffer containing 100 mM KCl and 10 mM ethyleneglycol tetraacetic acid (EGTA), pH 7.2, at 20 °C. The excitation wavelength was 595 nm. Fluorescence intensities at 609 nm of CaTM-3 in the presence of various concentrations of free Ca^{2+} were plotted against free Ca^{2+} concentrations. The dissociation constant K_d of CaTM-3 with Ca^{2+} was determined by curve fitting based on Eq. (2) with KaleidaGraph 4.1 (Synergy Software):

$$F = (F_{max}[Ca^{2+}]_{free} + F_{min}K_d)/([Ca^{2+}]_{free} + K_d) \quad (2)$$

where F is fluorescence intensity (a.u.); $[Ca^{2+}]_{free}$ is concentration of free Ca^{2+}.

2.5. Determination of apparent acid dissociation constants from absorbance change

Apparent acid dissociation constants of CaTM-3 were determined by the method previously reported [27]. Absorption spectra of 1 μM CaTM-3 were measured at 25 °C in 100 mM sodium phosphate buffer at various pH values, containing 1% DMSO as a cosolvent. A pH plot of normalized absorbance at 595 nm of CaTM-3 was made and curve fittings were done based on Eq. (3) with KaleidaGraph 4.1 (Synergy Software).

$$A = \frac{\left(A_{neutral} + 10^{pH-pK_{a1}} * A_{monoanion} + 10^{2pH-pK_{a1}-pK_{a2}} * A_{dianion}\right)}{\left(1 + 10^{pH-pK_{a1}} + 10^{2pH-pK_{a1}-pK_{a2}}\right)} \quad (3)$$

where A is normalized absorbance; $A_{neutral}$ is normalized absorbance for the neutral form; $A_{monoanion}$ is normalized absorbance for the monoanion form; $A_{dianion}$ is normalized absorbance for the dianion form. pK_{a1} and pK_{a2} are apparent acid dissociation constants for neutral-monoanion and for monoanion-dianion, respectively [27].

2.6. Preparation of cells

HeLa cells, COS7 cells, A549 cells, MCF-7 cells and NIH3T3 cells were cultured in Dulbecco's modified Eagle's medium (DMEM) (Invitrogen Corp.). HEK293 cells were cultured in DMEM supplemented with 1% MEM non-essential amino acid (Invitrogen Corp.) and 2 mM l-glutamine (Invitrogen Corp.), and CHO-k1 cells were cultured in Ham's F-12 (Wako). All cell lines were cultured in a humidified incubator containing 5% CO_2 in air. All media were supplemented with 10% (v/v) fetal bovine serum (Invitrogen Corp.), 1% penicillin and 1% streptomycin (Invitrogen Corp.).

2.7. General procedure of loading the dye for fluorescence imaging in cultured cells

HeLa cells, COS7 cells, A549 cells, and NIH3T3 cells were plated onto a 35-mm poly-D-lysine-coated glass-bottomed dish (MatTek) in DMEM supplemented with 10% (v/v) fetal bovine serum, 1% penicillin and 1% streptomycin. CHO-k1 cells were plated onto a 35-mm poly-D-lysine-coated glass-bottomed dish (MatTek) in Ham's F-12 supplemented with 10% (v/v) fetal bovine serum, 1% penicillin and 1% streptomycin. MCF-7 cells were plated onto a 35-mm poly-L-lysine-coated glass-bottomed dish (Matsunami) in DMEM supplemented with 10% (v/v) fetal bovine serum, 1% penicillin and 1% streptomycin. HEK293 cells were plated onto a 35-mm poly-D-lysine-coated glass-bottomed dish (MatTek) in DMEM supplemented with 1% MEM non-essential amino acid and 2 mM l-glutamine, 10% (v/v) fetal bovine serum, 1% penicillin and 1% streptomycin. Before loading dyes, the medium was removed and the cells were washed with Hanks' Balanced Salt Solution (HBSS) three times, then a fluorescent probe (CaTM-2 AM, CaTM-3 AM or Quest Rhod-4 AM) (3 μM) in HBSS containing 0.3% DMSO as a cosolvent was added to the cells. After incubation at 37 °C for 30 min, the medium was removed. The cells were washed with HBSS three times, and then observed in HBSS. For costaining with Quest Rhod-4 AM and MitoTracker Green, 3 μM Quest Rhod-4 AM was added

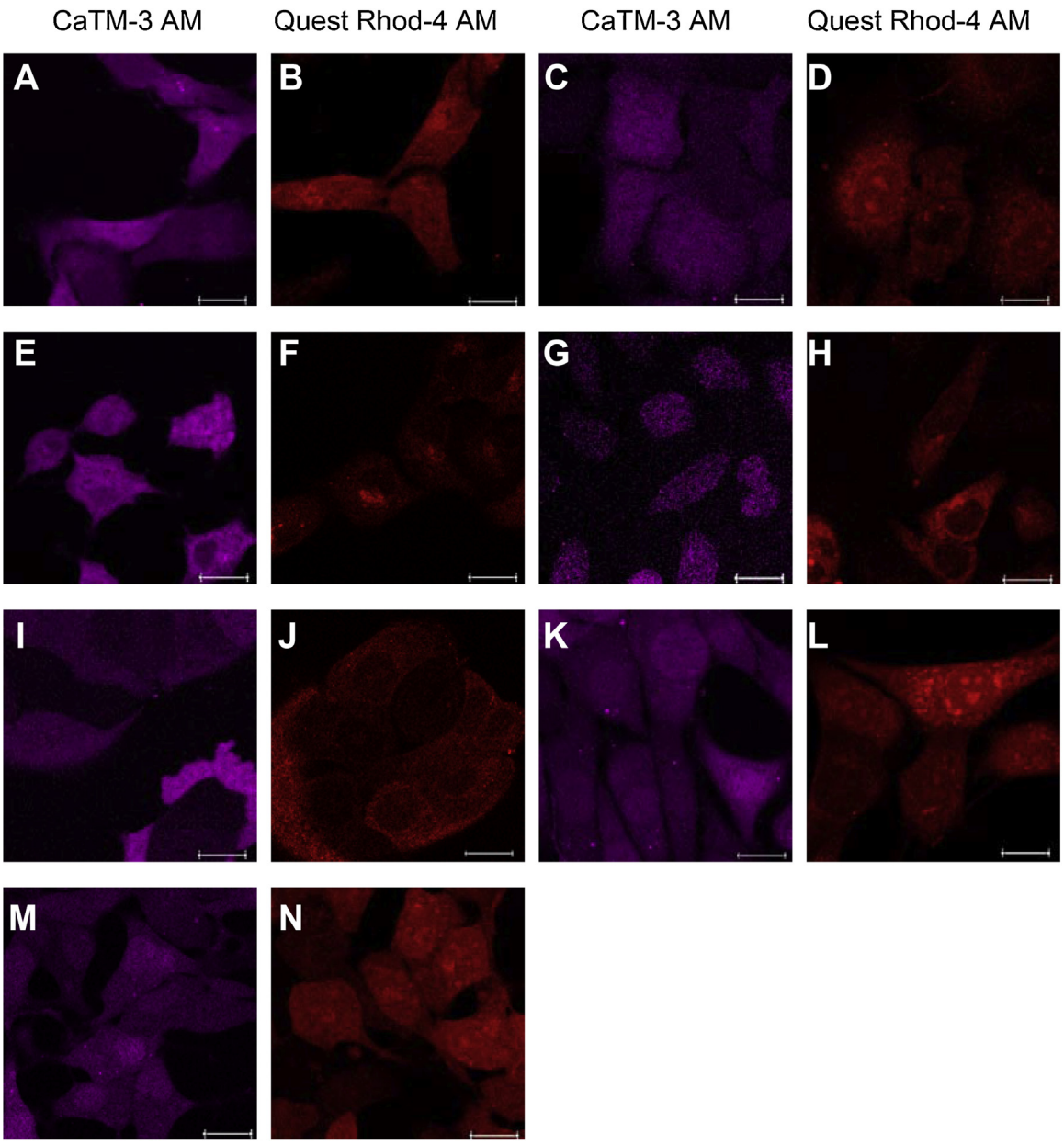

Fig. 4. Localizations of CaTM-3 AM and Quest Rhod-4 AM in living cells. HeLa cells (A,B), COS7 cells (C,D), A549 cells (E,F), CHO-k1 cells (G,H), MCF-7 cells (I,J), NIH3T3 cells (K,L) and HEK293 cells (M,N) were loaded with CaTM-3 AM (A,C,E,G,I,K,M) or QuestRhod-4 AM (B,D,F,H,J,L,N), and fluorescence images were captured. No specific localization of CaTM-3 inside cells was observed, except in the nucleus, in this experiment. On the other hand, QuestRhod-4 showed partial localization in mitochondria. Scale bars: 15 μm.

in the same procedure, and then the medium was replaced with 0.2 μM MitoTracker Green FM in HBSS. After incubation at 37 °C for 30 min, the medium was removed, and the cells were observed in HBSS. Medium was warmed at 37 °C before all procedures.

2.8. General procedure for conventional fluorescence imaging of cultured cells

The imaging system comprised an inverted microscope (IX 71; Olympus) and cooled CCD camera (CCD DR328G-C 01-SIL; Molecular Devices Inc.). The microscope was equipped with a xenon lamp (U-RX-T; Olympus) and a 40 × objective lens (UplanFL, N. A. 1.30 Oil; Olympus). The fluorescence mirror units were U-FMCHE (BP565-585 excitation filter, BA600-690 emission filter, DM595 Olympus) for CaTM-3 AM. The whole system was controlled with Metamorph software (Molecular Devices Inc.).

2.9. General procedure for confocal fluorescence imaging of cultured cells

A confocal imaging system (TCSSP5; Leica) equipped with a white light laser was used. Fluorescence images were captured with excitation and emission wavelengths of 590/610–680 nm for CaTM-2 AM, CaTM-3 AM and 530/550–600 nm for Quest Rhod-4 AM (AAT Bioquest). When cells were costained with Quest Rhod-4 AM and MitoTracker Green FM (Invitrogen Corp.), excitation and emission wavelengths were 490/505–520 nm for MitoTracker Green FM and 550/570–600 nm for Quest Rhod-4 AM.

2.10. Organotypic hippocampal slice cultures

All experimental procedures using animals were approved by the Animal Care and Use Committee of the University of Tokyo.

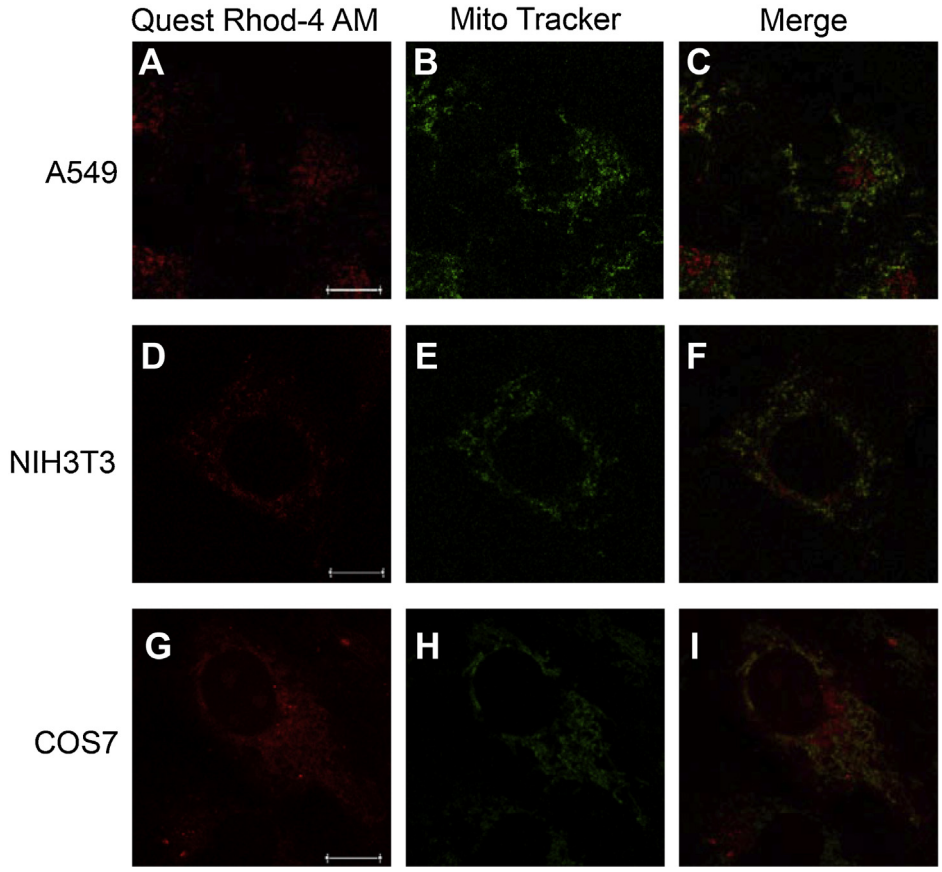

Fig. 5. Costaining with Quest Rhod-4 AM and MitoTracker. A549 cells (A–C), NIH3T3 cells (D–F) and COS7 cells (G–I) were loaded with QuestRhod-4 AM (3 μM) and MitoTracker Green FM (0.2 μM), then images were captured. Fluorescence images of Quest Rhod-4 AM (A,D,G), MitoTracker Green (B,E,H) and merged images (C,F,I) are shown. Signals from Quest Rhod-4 AM were partially merged with those of MitoTracker, demonstrating partial localization of Quest Rhod-4 AM into mitochondria in A549 cells, NIH3T3 cells and COS7 cells. Scale bars: 10 μm. (For interpretation of the references to colour in this figure legend, the reader is referred to the web version of this article.)

Hippocampal slices (300 μm thick) were prepared from postnatal day 7 Wistar/ST rats (SLC, Shizuoka, Japan), placed on an Omnipore membrane filter, and incubated with culture media in 5% CO_2 at 37 °C. They were maintained for 7 days *in vitro* and then used for experiments.

2.11. Dye loading and calcium imaging in slices

Slice cultures were incubated with 2 mL dye solution at 37 °C for 40 min. The dye solution was artificial cerebrospinal fluid (ACSF) containing 8 μM CaTM-3 AM, 0.01% Pluronic F-127, 0.005% Cremophor EL, and 0.08% DMSO as a cosolvent. ACSF consisted of (in mM): 127 NaCl, 26 $NaHCO_3$, 3.5 KCl, 1.24 NaH_2PO_4, 1.3 $MgSO_4$, 1.5 $CaCl_2$, and 10 glucose. After the incubation, the slices were washed with ACSF three times and allowed to recover in 2 mL ACSF at 37 °C for 45 min. For calcium imaging, slice cultures were transferred into a recording chamber heated at 35 °C and continuously perfused with ACSF at 2 mL/min. Images were acquired at 10 frames/sec with a Nipkow-disk confocal unit (CSUX-1, Yokogawa Electric, Tokyo, Japan), a CMOS camera (ORCA-Flash4.0 V2, Hamamatsu Photonics, Shizuoka, Japan), a water-immersion objective lens (16 ×, 0.80 NA, Nikon, Tokyo, Japan), and image acquisition software (HSR, Hamamatsu Photonics, Shizuoka, Japan). CaTM-3 was excited at 568 nm (15 mW) with an argon-krypton laser (641-YB-A01; Melles Griot, Carlsbad, CA, USA) and visualized using 617–673 nm band-pass emission filters. Data analysis was performed with custom software written in Microsoft Visual Basic. In each cell body, the fluorescence change $\Delta F/F$ was calculated as $(F_t - F_0)/F_0$, where F_t is the fluorescence intensity at frame time t, and F_0 is the average baseline.

3. Results

3.1. Design and synthesis of CaTM-3 and CaTM-3 AM

We designed and synthesized CaTM-3 as a new red fluorescent probe for Ca^{2+} (Fig. 1A), based on the 2-COOH DCTM scaffold (Fig. 1B). 2-COOH DCTM shows the suitable photophysical properties for biological applications ($\Phi_f = 0.48$, $\varepsilon_{591} = 1.2 \times 10^5\ cm^{-1}\ M^{-1}$), like fluorescein ($\Phi_f = 0.85$, $\varepsilon_{490} = 8.8 \times 10^4\ cm^{-1}\ M^{-1}$), which is used as a parent fluorophore for green fluorescent probes for Ca^{2+} such as Calcium Green-1 and Oregon Green 488 BAPTA-1 [16,17,27]. We also examined the photobleaching of 2-COOH DCTM and fluorescein (Fig. 1C). The results showed that 2-COOH DCTM is more stable than fluorescein under light irradiation. In the molecular design of CaTM-3, the 1,2-bis(*o*-aminophenoxy)ethane-*N*,*N*,*N*′,*N*′-tetraacetic acid (BAPTA) moiety, which is a selective chelator of Ca^{2+} among physiological metal ions, including Mg^{2+}, was conjugated to the benzene moiety of 2-COOH DCTM via an amide bond (Fig. 1A), as in Calcium Green-1 and Oregon Green 488 BAPTA-1 [16,17]. CaTM-3 was synthesized via a modification of the scheme used for CaTM-2 [26,29]. For cellular applications, we also synthesized CaTM-3 AM, an AM ester form of CaTM-3 (Fig. 1A) [29]. Because of the hydrophilicity of the BAPTA moiety, Ca^{2+} indicators generally cannot pass through cell membranes without the use of special

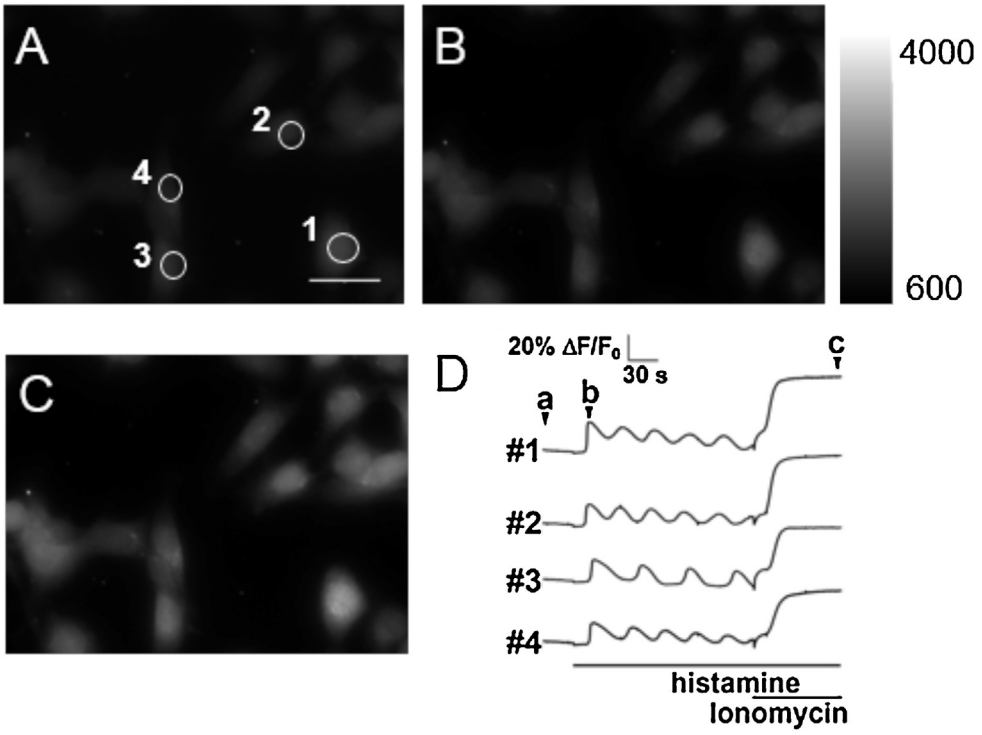

Fig. 6. Fluorescence imaging of histamine-induced calcium oscillations in HeLa cells utilizing CaTM-3 AM. HeLa cells were incubated with 3 μM CaTM-3 AM in HBSS buffer containing 0.3% DMSO at 37 °C for 30 min. Then, the dyes were washed out three times and fluorescence imaging was started. Cells were stimulated with histamine (1 μM) at 30 s and ionomycin (5 μM) at 210 s. A-C. Fluorescence images at the time points indicated in D. D. Fluorescence intensity changes in ROIs of individual cells numbered 1–4. Exposure time was 100 msec and the ND filter was 25%. The images were captured with excitation and emission wavelengths of 565–585/600–690 nm. Scale bar in A: 20 μm.

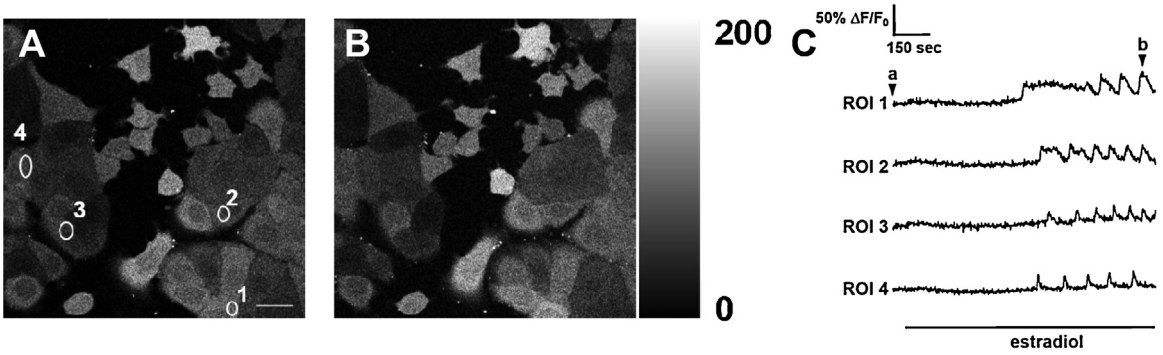

Fig. 7. Fluorescence imaging of estradiol-induced calcium oscillations in MCF-7 cells utilizing CaTM-3 AM. MCF-7 cells were incubated with 3 μM CaTM-3 AM in HBSS buffer containing 0.3% DMSO at 37 °C for 30 min. Then, the dyes were washed out three times and fluorescence imaging was started. Cells were stimulated with estradiol (1 μM) at 60 s. A,B. Fluorescence images at the time points indicated in C. C. The fluorescence intensity change in ROIs of individual cells numbered 1–4. The images were captured with excitation and emission wavelengths of 590/610–680 nm. Scale bars: 30 μm.

procedures, such as electroporation or the beads-loading method [30,31]. In contrast, AM ester forms of Ca^{2+} probes can readily enter cells, where they are enzymatically cleaved by intracellular esterase to afford the Ca^{2+}-sensitive, cell-impermeable form.

3.2. *Ca^{2+}-dependent photophysical properties of CaTM-3*

To evaluate the applicability of CaTM-3 as a red fluorescent probe for Ca^{2+}, we next examined the absorption and emission spectra of CaTM-3 before and after addition of Ca^{2+} (Fig. 2A and B). The absorption spectrum of CaTM-3 did not change upon addition of Ca^{2+} (Fig. 2A), but on the other hand, an 8-fold fluorescence increase was observed (Fig. 2B). The dissociation constant K_d of CaTM-3 with Ca^{2+} was also determined from the changes of the fluorescence intensity of CaTM-3 at 609 nm in the presence of various concentrations of free Ca^{2+} (Fig. 2C), and the K_d was calculated to be 0.19 μM, which is the same as that of the commercially available green fluorescent probe, Calcium Green-1 (K_d = 0.19 μM) [17]. Moreover, the maximum wavelengths of absorption (λ_{abs}) and emission (λ_{em}), fluorescence quantum yield (Φ_{fl}) and dissociation constant of CaTM-3 were almost the same as those of CaTM-2, and are suitable for biological applications (Table 1). We next examined the absorption spectral change of CaTM-3 at various pH values (Fig. 2D and E). Interestingly, the absorption change of CaTM-3 occurred under more acidic conditions (pK_{a1} = 6.8 and pK_{a2} = 5.8) than in the case of its fluorophore scaffold, 2-COOH DCTM (pK_{a1} = 7.0 and pK_{a2} = 6.2) [27]. Thus, CaTM-3 exists mainly in the strongly fluorescent dianion form at physiological pH (pH 7.4), as shown in Fig. 2F. These properties indicate that CaTM-3 would be practically useful as a fluorescent probe for Ca^{2+} *in vitro* assay.

Table 1
Ca^{2+}-dependent photophysical properties of CaTM-2 and CaTM-3.

	λ_{abs} (nm)[a]	λ_{em} (nm)[a]	Φ_{fl}[a,b]	K_d (μM)[a]
CaTM−2[c]	597	609	0.024	–
+ Ca^{2+}[d]	597	609	0.39	0.20
CaTM−3[c]	595	609	0.046	–
+ Ca^{2+}[d]	595	609	0.37	0.19

[a] Measured in 30 mM MOPS buffer containing 100 mM KCl and 10 mM EGTA, pH 7.2, 20 °C.
[b] Fluorescence quantum yields were calculated using that of TokyoMagenta (Φ_{fl} = 0.42) in 100 mM sodium phosphate buffer (pH 9.0) as a standard [28].
[c] Measured in 0 μM free Ca^{2+}.
[d] Measured in 39 μM free Ca^{2+}. The data of CaTM-2 were cited from reference 26.

3.3. Cellular applications of CaTM-3 AM

To examine the efficiency of probe loading into cells, we loaded HeLa cells with CaTM-2 AM or CaTM-3 AM and captured fluorescence images. In the case of CaTM-2 AM, aggregates of the probe were observed as strongly fluorescent dots (Fig. 3A). On the other hand, stronger fluorescence was observed uniformly in the cells without aggregation in the case of CaTM-3 AM (Fig. 3B). CaTM-3 was distributed to the cytosol and the nucleus, like Fluo-3, Fluo-4, Calcium Green-1 and Oregon Green 488 BAPTA-1 [32]. We further examined the intracellular localization of CaTM-3 AM in other cell lines (COS7, A549, CHO-k1, MCF-7, NIH3T3 and HEK293) (Fig. 4). No distinctive compartmentalization of CaTM-3 AM inside these cells was observed, in contrast to the mitochondrial localization of Rhod-2 AM [33–35]. We further compared the usefulness of CaTM-3 AM as a red cytosolic fluorescent probe with that of Quest Rhod-4 AM (AAT Bioquest, Sunnyvale, CA), which was recently commercialized as an improved Rhod-2 AM that exhibits cytosolic distribution inside cells. We examined the intracellular localization of Quest Rhod-4 AM, as well as CaTM-3 AM, in various living cells (HeLa, COS7, A549, CHO-k1, MCF-7, NIH3T3 and HEK293) (Fig. 4). We found that Quest Rhod-4 AM is basically distributed to the cytosol, but it also shows some mitochondrial localization in NIH3T3, A549 and COS7 cells (Fig. 5), whereas CaTM-3 AM was mainly localized in the cytosol, except for the nucleus. Thus, CaTM-3 AM should be useful for monitoring cytoplasmic Ca^{2+} concentration in the red color region.

Next, we examined whether CaTM-3 AM can detect physiological changes in intracellular cytoplasmic Ca^{2+} concentration with a conventional fluorescence imaging system (Fig. 6). HeLa cells were loaded with CaTM-3 AM and then stimulated with histamine to induce Ca^{2+} oscillation [36]. The Ca^{2+} ionophore, ionomycin, was further added to the cells to increase the intracellular Ca^{2+} concentration [37]. We found that CaTM-3 AM could visualize physiological changes in cytoplasmic Ca^{2+} concentration (Fig. 6D; see also supplemental Movie 1). We also examined whether CaTM-3 AM could be used with a confocal fluorescence imaging system. The intracellular cytoplasmic Ca^{2+} concentration change in MCF-7 cells after stimulation with estradiol or G-1, which is a GPR30-selective high-affinity ligand, was successfully monitored (Fig. 7 and Fig. 8; see also Supplemental Movies 2,3) [38,39].

3.4. Applications of CaTM-3 AM to brain slices

Fluorescence imaging of Ca^{2+} has been used in neuroscience for the analysis of neuronal networks in terms of increases in somatic Ca^{2+} following neuronal action potentials [40–45]. Therefore, we examined whether CaTM-3 AM could be used to monitor the activity of neurons in cultures of rat hippocampal slices (Fig. 9). Interestingly, when we bulk-loaded a culture of rat hippocampal slices with CaTM-3 AM by the incubation method, the probe showed much higher loading efficiency into neurons than did CaTM-2 AM. Moreover, spontaneous neuronal firing could be observed in terms of somatic changes in the fluorescence intensity of CaTM-3 (Fig. 9A and B; see also supplemental Movie 4). We noted simultaneous activation of plural neurons. Then, we employed this probe to visualize the action-potential-mediated Ca^{2+} increase in the neuronal cell body. Neurons were loaded with CaTM-3 AM by the incubation method, and action potentials were evoked with brief current injections. The amplitude of the fluorescence change was positively correlated with the number of action potentials, allowing the number of action potentials to be estimated (Fig. 9C).

4. Discussion

The development of practical fluorescent probes has greatly contributed to elucidation of the molecular mechanisms of many complex biological phenomena, including those related to the Ca^{2+} signaling [1–12]. Currently used small-molecular fluorescent probes for Ca^{2+} are mostly fluorescein derivatives, such as Fluo-3, Fluo-4, Calcium Green-1 and Oregon Green 488 BAPTA-1, and emit green fluorescence (ca. 527 nm) [15–17].

For further biological applications of Ca^{2+} indicators, e.g., in multicolor imaging and *in vivo* imaging, red to NIR fluorescent probes are required, and several have recently been reported [20]. These probes have various advantages and disadvantages: for example, Quest Rhod-4 AM is a commercially available red-fluorescent Ca^{2+} probe, which is superior in brightness to Rhod-2 AM and shows cytosolic localization inside cells, unlike Rhod-2 AM. However, its absorption and emission wavelengths both lie in a similar wavelength region ($\lambda_{abs,max}$ = 530 nm, $\lambda_{em,max}$ = 555 nm) and it shows partial mitochondrial localization in NIH3T3, A549 and COS7 cells (Fig. 5). We previously developed CaSiR-1 AM as a NIR fluorescent probe for Ca^{2+}, and showed that it is practically useful for neuronal Ca^{2+} imaging [23,45], but it was localized in lysosomes in some cultured cells [26]. KFCA is also a NIR fluorescent probe for Ca^{2+}, and has been used to monitor cytoplasmic Ca^{2+} concentration [24]. However, it had to be introduced into cells by bead-loading [31]. More recently, CaRuby-Nano [46] has been reported as a red fluorescent probe for Ca^{2+}, together with Calcium Rubies [22,25], which has submicromolar affinity for Ca^{2+}. An AM-ester form of Calcium Rubies was conjugated to dextrans for biological applications [20]. Our previous red Ca^{2+} probe, CaTM-2 AM, could also be used to monitor cytoplasmic Ca^{2+} concentrations in cultured cells and neuronal activity in cultures of rat hippocampal slices [26], but showed relatively poor introduction efficiency into live cells.

As described above, our new probe, CaTM-3 AM, has suitable photophysical properties for biological applications, though the fluorescence enhancement (8-fold) of CaTM-3 is smaller than that of CaTM-2 (16-fold) (Table 1). Among representative small-molecular green fluorescent probes for Ca^{2+}, Fluo-3 and Fluo-4 are almost nonfluorescent in the absence of Ca^{2+} and exhibit approximately a 100-fold fluorescence increase upon Ca^{2+} binding, affording a very large dynamic range [17]. On the other hand, although Calcium Green-1 and Oregon Green 488 BAPTA-1 exhibit weaker fluorescence enhancement (14-fold), they show fluorescence even in resting cells, unlike Fluo-3 and Fluo-4. So, Calcium Green-1 and Oregon Green 488 BAPTA-1 increase the visibility of unstimulated cells. They also facilitate the determination of baseline fluorescence and make monitoring of intracellular Ca^{2+} concentrations more reliable [17]; consequently, they have been employed for imaging of multiple neurons in neurosciences [40,43,44]. The photophysical properties of CaTM-3 are similar to those of Calcium Green-1 and Oregon Green 488 BAPTA-1, but not Fluo-3 and Fluo-4, in terms of the moderate fluorescence quantum yield (0.046) in the absence of Ca^{2+} and the K_d with Ca^{2+} (Calcium Green-1: K_d = 0.19 μM) [17]; this is probably due to the similarity of chemical structure between

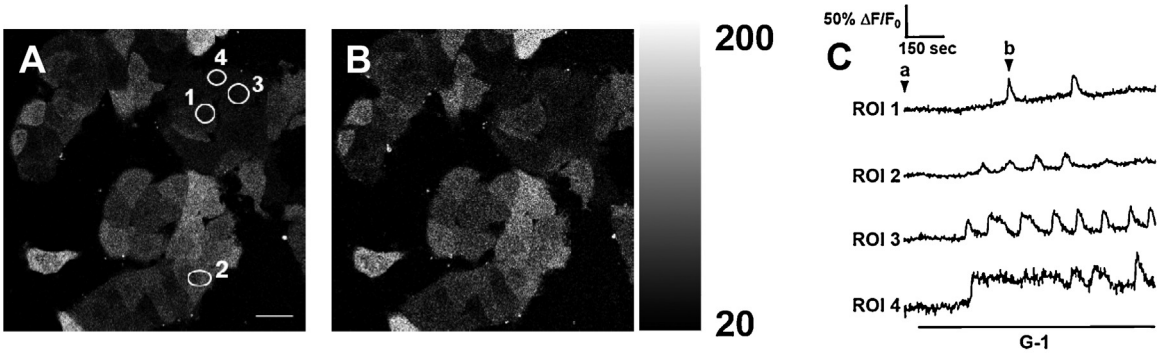

Fig. 8. Fluorescence imaging of G-1-induced calcium oscillations in MCF-7 cells utilizing CaTM-3 AM. G-1 is a GPR30-selective high-affinity ligand [38,39]. MCF-7 cells were incubated with 3 μM CaTM-3 AM in HBSS buffer containing 0.3% DMSO at 37 °C for 30 min. Then, the dyes were washed out three times and fluorescence imaging was started. Cells were stimulated with G-1 (1 μM) at 60 s. A,B. Fluorescence images at the time points indicated in C. C. Fluorescence intensity change in ROIs of individual cells numbered 1–4. The images were captured with excitation and emission wavelengths of 590/610–680 nm. Scale bars: 30 μm.

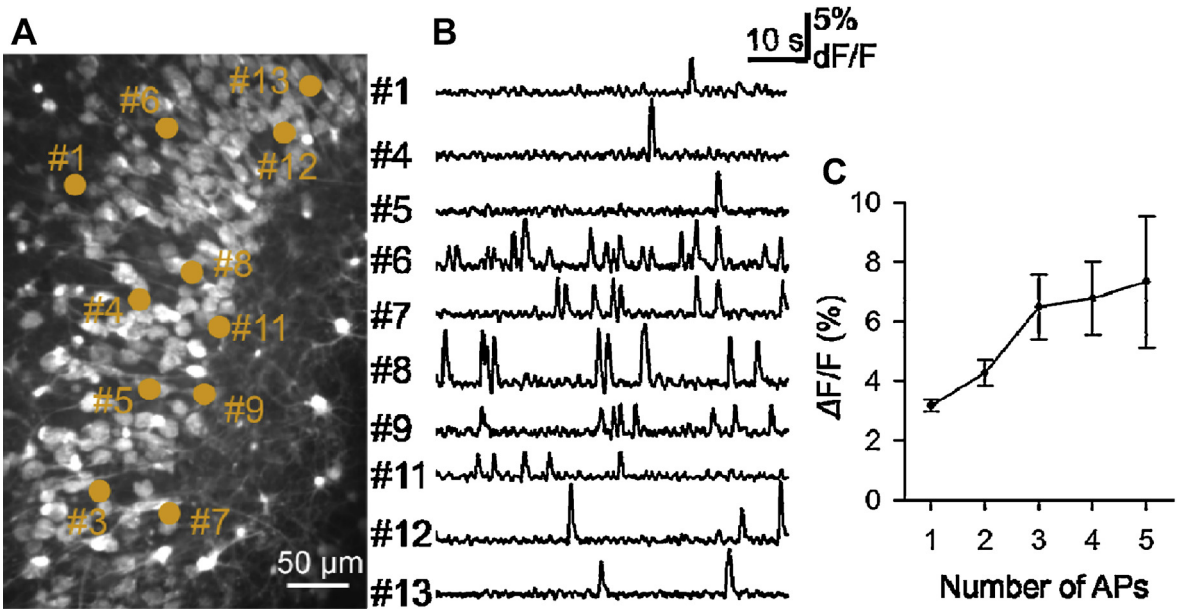

Fig. 9. Application of CaTM-3 AM to monitor the activity of neurons. A. A fluorescence image of the CA3 pyramidal cell layer in a hippocampal slice culture after incubation with CaTM-3 AM. B. Spontaneous calcium activities in the neurons numbered in A. Images were monitored at 10 frames per second. C. Relationship of the ΔF/F response amplitude to the number of action potentials. Action potentials were recorded in the patch-clamp cell-attached configuration. Action potentials were elicited by electrical field stimulation of axonal fibers. Images were monitored at 100 frames per sec. n = 3-9 trials from 2 to 6 neurons. Data represent mean ± s.e.m.

CaTM-3 and Calcium Green-1 or Oregon Green 488 BAPTA-1 [17]. Further, CaTM-3 AM shows higher introduction efficiency into the cells than does CaTM-2 AM, probably because its hydrophilicity is greatly improved by introducing a carboxy group into the probe structure. CaTM-3 AM was also distributed into the cytosol and the nucleus in the same way as typical green Ca^{2+} fluorescent probes: Fluo-3, Fluo-4, Calcium Green-1 and Oregon Green 488 BAPTA-1 [32]. Furthermore, it could be applied to fluorescence imaging of physiological Ca^{2+} concentration changes in not only live cells, but also brain slices. From all these results, CaTM-3 AM appears to be a potential red-colored substitute for Calcium Green-1 AM and Oregon Green 488 BAPTA-1 AM.

In conclusion, in this study, we focused on improving the water solubility of CaTM-2 AM, and developed CaTM-3 AM as a practical red-fluorescent probe for monitoring cytoplasmic Ca^{2+}, with high cell-membrane permeability and bright fluorescence. We confirmed its usefulness in biological applications in cultured cells and hippocampal slice cultures with conventional and confocal fluorescence imaging systems. Because changes in cytoplasmic concentration of Ca^{2+} are deeply related to various physiological phenomena, simultaneous monitoring of cytoplasmic Ca^{2+} and other metal ions, proteins or biomolecules is important for detailed analysis of biological molecular mechanisms. CaTM-3 AM could be utilized in combination with various fluorophores that emit in the UV to yellow range: for example, it would be applicable in GFP-expressing animals and cultured cells. We believe that this probe will open up new possibilities for innovative approaches to a variety of Ca^{2+}-related research problems.

Acknowledgements

We are very grateful for the valuable advice of Prof. Tomoya Hirano from Tokyo Medical and Dental University. This work was supported in parts by MEXT (Specially Promoted Research Grant Nos. 22000006 to T.N., Grant Nos. 24689003, 24659042 and 26104509 to K.Hanaoka, and Grant Nos. 24655147 to T.K.), and SENTAN, JST to K.Hanaoka. K.Hanaoka was also supported by Mochida Memorial Foundation for Medical and Pharmaceutical Research, The Asahi Glass Foundation, Takeda Science Foundation and The

Cosmetology Research Foundation. K.Hirabayashi was supported by a Grant-in-Aid for JSPS Fellows.

Appendix A. Supplementary data

Supplementary data associated with this article can be found, in the online version, at http://dx.doi.org/10.1016/j.ceca.2016.06.002.

References

[1] A.P. de Silva, H.Q.N. Gunaratne, T. Gunnlaugsson, et al., Signaling recognition events with fluorescent sensors and switches, Chem. Rev. 97 (1997) 1515–1566.
[2] G. Zlokarnik, P.A. Negulescu, T.E. Knapp, et al., Quantitation of transcription and clonal selection of single living cells with β-lactamase as reporter, Science 279 (1998) 84–88.
[3] T. Nagano, T. Yoshimura, Bioimaging of nitric oxide, Chem. Rev. 102 (2002) 1235–1269.
[4] T. Terai, T. Nagano, Fluorescent probes for bioimaging applications, Curr. Opin. Chem. Biol. 12 (2008) 515–521.
[5] G. Grynkiewicz, M. Poenie, R.Y. Tsien, A new generation of Ca^{2+} indicators with greatly improved fluorescence properties, J. Biol. Chem. 260 (1985) 3440–3450.
[6] A.T. Harootunian, J.P.Y. Kao, S. Paranjape, R.Y. Tsien, Generation of calcium oscillations in fibroblasts by positive feedback between calcium and IP3, Science 251 (1991) 75–78.
[7] J. Hambers, R.S. Ames, D. Bergsma, et al., Melanin-concentrating hormone is the cognate ligand for the orphan G-protein coupled receptor SLC-1, Nature 400 (1999) 261–265.
[8] I. Micu, A. Ridsdale, L. Zhang, et al., Real-time measurement of free Ca^{2+} changes in CNS myelin by two-photon microscopy, Nat. Med. 13 (2007) 874–879.
[9] D. Skokos, G. Shakhar, R. Varma, et al., Peptide-MHC potency governs dynamic interactions between T cells and dendritic cells in lymph nodes, Nat. Immunol. 8 (2007) 835–844.
[10] K.V. Kuchibhotla, C.R. Lattarulo, B.T. Hyman, B.J. Bacskai, Synchronous hyperactivity and intercellular calcium waves in astrocytes in alzheimer mice, Science 323 (2009) 1211–1215.
[11] M.J. Berridge, M.D. Bootman, H.L. Roderick, Calcium signaling: dynamics, homeostasis and remodeling, Nat. Rev. Mol. Cell. Biol. 4 (2003) 517–529.
[12] D.E. Clapham, Calcium signaling, Cell 131 (2007) 1047–1058.
[13] A. Miyawaki, J. Llopis, R. Heim, et al., Fluorescent indicators for Ca^{2+} based on green fluorescent proteins and calmodulin, Nature 388 (1997) 882–887.
[14] Y. Zhao, S. Araki, J. Wu, et al., An expanded palette of genetically encoded Ca^{2+} indicators, Science 333 (2011) 1888–1891.
[15] A. Minta, J.P.Y. Kao, R.Y. Tsien, Fluorescent indicators for cytosolic calcium based on rhodamine and fluorescein chromophores, J. Biol. Chem. 264 (1989) 8171–8178.
[16] Monitoring cell calcium, in: R.Y. Tsien, E. Carafoli, C. Klee (Eds.), Calcium as a Cellular Regulator, Oxford University Press, New York, 1999, pp. 28–54.
[17] The Molecular Probes Handbook: A Guide to Fluorescent Probes and Labeling Technologies, 11th ed, (I. Johnson, M.T.Z. Spence, eds.), Life Technologies, Eugene, OR (2010).
[18] S.M. Ward, T. Ördög, S.D. Koh, et al., Pacemaking in interstitial cells of Cajal depends upon calcium handling by endoplasmic reticulum and mitochondria, J. Physiol. 525 (2000) 355–361.
[19] J.P.Y. Kao, G. Li, D.A. Auston, Practical aspects of measuring intracellular calcium signals with fluorescent indicators, Methods Cell Biol. 99 (2010) 113–152.
[20] M. Oheim, M. van't Hoff, A. Feltz, A. Zamaleeva, J.-M. Mallet, M. Collot, New red-fluorescent calcium indicators for optogenetics, photoactivation and multi-color imaging, Biochim. Biophys. Acta 1843 (2014) 2284–2306.
[21] S. Bolsover, O. Ibrahim, N. Oluanaigh, H. Williams, S. Cockcroft, Use of fluorescent Ca^{2+} dyes with green fluorescent protein and its variants: problems and solutions, Biochem. J. 356 (2001) 345–352.
[22] C. Luccardini, A.V. Yakovlev, M. Pasche, et al., Measuring mitochondrial and cytoplasmic Ca^{2+} in EGFP expressing cells with a low-affinity Calcium Ruby and its dextran conjugate, Cell Calcium 45 (2009) 275–283.
[23] T. Egawa, K. Hanaoka, Y. Koide, et al., Development of a far-red to near-infrared fluorescence probe for calcium ion and its application to multicolor neuronal imaging, J. Am. Chem. Soc. 133 (2011) 14157–14159.
[24] A. Matsui, K. Umezawa, Y. Shindo, et al., A near-infrared fluorescent calcium probe: a new tool for intracellular multicolour Ca^{2+} imaging, Chem. Commun. 47 (2011) 10407–10409.
[25] M. Collot, C. Loukou, A.V. Yakovlev, et al., Calcium rubies: a family of red-emitting functionalizable indicators suitable for two-photon Ca^{2+} imaging, J. Am. Chem. Soc. 134 (2012) 14923–14931.
[26] T. Egawa, K. Hirabayashi, Y. Koide, et al., Red fluorescent probe for monitoring the dynamics of cytoplasmic calcium ions, Angew. Chem. Int. Ed. 52 (2013) 3874–3877.
[27] K. Hirabayashi, K. Hanaoka, T. Takayanagi, et al., Analysis of chemical equilibrium of Si-substituted fluorescein and its application to develop a scaffold for red fluorescent probes, Anal. Chem. 87 (2015) 9061–9069.
[28] T. Egawa, Y. Koide, K. Hanaoka, T. Komatsu, T. Terai, T. Nagano, Development of a fluorescein analogue TokyoMagenta, as a novel scaffold for fluorescence probes in red region, Chem. Commun. 47 (2011) 4162–4164.
[29] K. Hirabayashi, K. Hanaoka, T. Egawa, et al. Synthesis of Practical Red Fluorescent Probe for Cytoplasmic Calcium Ions with Greatly Improved Cell-membrane Permeability Data in Brief, submitted.
[30] W. Göbel, F. Helmchen, In vivo calcium imaging of neural network function, Physiology 22 (2007) 358–365.
[31] P.L. McNeil, E. Warder, Glass beads load macromolecules into living cells, J.Cell Sci. 88 (1987) 669–678.
[32] D. Thomas, S.C. Tovey, T.J. Collins, M.D. Bootman, M.J. Berridge, P. Lipp, A comparison of fluorescent Ca^{2+} indicator properties and their use in measuring elementary and global Ca^{2+} signals, Cell Calcium 28 (2000) 213–223.
[33] G. Hajnóczky, L.D. Robb-Gaspers, M.B. Seitz, A.P. Thomas, Decoding of cytosolic calcium oscillations in the mitochondria, Cell 82 (1995) 415–424.
[34] T.J. Collins, P. Lipp, M.J. Berridge, M.D. Bootman, Mitochondrial Ca^{2+} uptake depends on the spatial and temporal profile of cytosolic Ca^{2+} signals, J. Biol. Chem. 276 (2001) 26411–26420.
[35] M.J. Jou, T.I. Peng, S.S. Sheu, Histamine induces oscillations of mitochondrial free Ca^{2+} concentration in single cultured rat brain astrocytes, J. Physiol. 497 (1996) 299–308.
[36] D.M. Zhu, E. Tekle, C.Y. Huang, P.B. Chock, Inositol tetrakisphosphate as a frequency regulator in calcium oscillations in HeLa cells, J. Biol. Chem. 275 (2000) 6063–6066.
[37] G.J.J. Stege, P.K. Wierenga, H.H. Kampinga, A.W. Konings, Hyperthermia, intracellular free calcium and calcium ionophores, J. Radiat. Biol. 64 (1993) 459–468.
[38] T. Improta-Brears, A.R. Whorton, F. Codazzi, J.D. York, T. Meyer, D.P. McDonnell, Estrogen-induced activation of mitogen-activated protein kinase requires mobilization of intracellular calcium, Proc. Natl. Acad. Sci. U. S. A. 96 (1999) 4686–4691.
[39] E.A. Ariazi, E. Brailoiu, S. Yerrum, et al., The G protein?coupled receptor GPR30 inhibits proliferation of estrogen receptor?positive breast cancer cells, Cancer Res. 70 (2010) 1184–1194.
[40] D.A. Dombeck, A.N. Khabbaz, F. Collman, T.L. Adelman, D.W. Tank, Imaging large-scale neural activity with cellular resolution in awake, mobile mice, Neuron 56 (2007) 43–57.
[41] R. Cossart, D. Aronov, R. Yuste, Attractor dynamics of network UP states in the neocortex, Nature 423 (2003) 283–288.
[42] Y. Ikegaya, G. Aaron, R. Cossart, et al., Synfire chains and cortical songs: temporal modules of cortical activity, Science 304 (2004) 559–564.
[43] Z.F. Mainen, R. Malinow, K. Svoboda, Synaptic calcium transients in single spines indicate that NMDA receptors are not saturated, Nature 399 (1999) 151–155.
[44] Y. Kovalchuk, J. Eilers, J. Lisman, A. Konnerth, NMDA receptor-mediated subthreshold Ca^{2+} signals in spines of hippocampal neurons, J. Neurosci. 20 (2000) 1791–1799.
[45] M. Mizunuma, H. Norimoto, K. Tao, et al., Unbalanced excitability underlies offline reactivation of behaviorally activated neurons, Nat. Neurosci. 17 (2014) 503–505.
[46] M. Collot, C.D. Wilms, A. Bentkhayet, et al., CaRuby-Nano: a novel high affinity calcium probe for dual color imaging, eLIFE 4 (2015), UNSP e05808.